Available online at www.sciencedirect.com

ScienceDirect

Ciência & Tecnologia dos Materiais 25 (2013) 31–37

Ciência & Tecnologia dos MATERIAIS

http://ees.elsevier.com/ctmat

Special Issue on Polymers and Composites

Adhesive joints in natural fibre composites: estimation of fracture properties

R.D.S.G. Campilho[a,*], D.C. Moura[b], D.J.S. Gonçalves[b]

[a]*Departamento de Engenharia Mecânica, Instituto Superior de Engenharia do Porto, Instituto Politécnico do Porto, Rua Dr. António Bernardino de Almeida, 431, 4200-072 Porto, Portugal*

[b]*Faculdade de Engenharia da Universidade do Porto, Rua Dr. Roberto Frias, 4200-465 Porto, Portugal*

Abstract

Adhesive bonding has become more efficient in the last few decades due to the adhesives developments, granting higher strength and ductility. On the other hand, natural fibre composites have recently gained interest due to the low cost and density. It is therefore essential to predict the fracture behavior of joints between these materials. In this work, the tensile fracture toughness (G_n^c) of adhesive joints between natural fibre composites is studied, by bonding with a ductile adhesive and co-curing. Conventional methods to obtain Gnc are used for the co-cured specimens, while for the adhesive within the bonded joint, the *J*-integral is considered. For the *J*-integral calculation, an optical measurement method is developed for the evaluation of the crack tip opening and adherends rotation at the crack tip during the test, supported by a Matlab sub-routine for the automated extraction of these quantities. As output of this work, an optical method that allows an easier and quicker extraction of the parameters to obtain G_n^c than the available methods is proposed (by the *J*-integral technique), and the fracture behaviour in tension of bonded and co-cured joints in jute-reinforced natural fibre composites is also provided for the subsequent strength prediction. Additionally, for the adhesively-bonded joints, the tensile cohesive law of the adhesive is derived by the direct method.

Keywords: natural fibres; structural adhesives; fracture toughness; bonded joints.

1. Introduction

The developments in adhesives technology made possible the use of adhesive bonding in many fields of engineering, such as automotive and aeronautical, because of higher peel and shear strengths, and ductility. As a result, bonded joints are replacing fastening or riveting [1]. More uniform stress fields, capability of fluid sealing, high fatigue resistance and the possibility to join different materials are other advantages of adhesive bonding. However, stress concentrations exist in bonded joints along the bond length [2]. A large amount of works addresses the critical factors affecting the integrity of adhesive joints, such as the parent structure thickness, adhesive thickness, bonding length and geometric modifications that reduce stress concentrations [3]. On the other hand, natural fibre composites have recently gained interest, for instance in the construction or automotive industries, due to the low cost and density [4]. Thus, it is highly important the study of adhesive joints between these materials, to assess the feasibility of joining during the fabrication process of components (e.g. due to complex geometries), of joining cured parts of a structure or even for repairing purposes. Natural fibres like flax, henequen, sisal, coconut, jute, palm, bamboo, wood or paper have been used as reinforcement in thermosetting and thermoplastic resin composites [5]. Compared to typical fibre composites, e.g. with glass or carbon fibres, natural fibres benefit from lower density, less machining wear during fabrication, no health hazards,

* Corresponding author.

E-mail address: raulcampilho@gmail.com (R.D.S.G. Campilho)

http://dx.doi.org/10.1016/j.ctmat.2013.12.007

biodegradability, availability from natural and renewable sources and, most importantly, they are cheaper per unit volume basis [6]. However, their specific stiffness and strength do not match artificial fibres, and they suffer from high moisture absorption and poor wettability to some resins. The most commonly used matrix materials are polypropylene, polyester, polyurethane and epoxy. Most of the components made of natural fibre composites are fabricated by press-moulding, even though other processes are available [7].

The strength and failure mechanisms of bonded joints between these materials must be completely understood. The Finite Element Method (FEM) is the most accepted technique for the numerical strength prediction of bonded joints [8] by the calculation of stress and displacement fields, and combination with suitable failure criteria. Cohesive Zone Models (CZM), for instance, enable accurate fracture growth predictions [9]. CZM rely in the definition of the cohesive strength in tension and shear, t_n^0 and t_s^0, respectively (relating to the end of the elastic regime and beginning of damage), and the fracture toughness in tension and shear, G_n^c and G_s^c respectively (accounting for failure). A few methods are available to estimate the cohesive parameters and the respective laws: the property identification and inverse methods consist on assuming a simplified shape (bilinear or trilinear) for the fracture laws and estimation of the respective parameters by standardized procedures, while the direct method defines the precise law shape [10]. This is accomplished by the differentiation of the strain energy release rate in tension (G_n) or shear (G_s) with respect to the relative opening (δ_n for tension or δ_s for shear). Carlberger and Stigh [11] estimated the cohesive laws of an layer adhesive in tension and shear by the direct method, using the Double-Cantilever Beam (DCB) and End-Notched Flexure (ENF) tests, respectively, considering $0.1 \leq t_A \leq 1.6$ mm (t_A is the adhesive thickness). The cohesive laws were estimated by differentiation of the *J*-integral vs. crack tip opening data, obtained from physical sensors.

This work evaluates the tensile fracture behaviour of adhesive joints between natural fibre composites, considering adhesively-bonding with a ductile polyurethane adhesive and co-curing. Conventional methods are used to obtain G_n^c for the co-cured specimens, while for the adhesively-bonded joints, the *J*-integral is selected to account for the plasticity effects. For the *J*-integral, an automated optical measurement method is used for the evaluation of crack tip opening and adherends rotation at the crack tip, supported by a Matlab routine. Additionally, for the adhesively-bonded joints, the tensile cohesive law of the adhesive is derived by the direct method.

2. Experimental work

2.1. Materials

The adherends used in this work consist of a jute-epoxy composite, with jute weave as reinforcement. The use of jute is related to the attractive strength and toughness properties of this reinforcement material (between 1/8 and 1/4 of *E*-glass fibres; [12]), and higher stiffness than other natural fibres such as Sisal [13]. Moreover, the specific gravity of jute is nearly half that of glass fibres (≈1.3 compared to ≈2.5), which makes it a viable replacement, allowing to match the stiffness of glass fibre components at a smaller weight (the stiffness of jute fibres is nearly 80% that of glass fibres [14]) and cost (the cost per weight of jute may achieve 1/9 that of glass fibres). Typical properties of jute are as follows: density of 1.3-1.4 g/cm^3, elongation at failure of 1.5-1.8%, tensile strength of 400-800 MPa and Young's modulus (E) of 15-30 GPa. Epoxy was chosen for the matrix material on account of the good mechanical (strength and stiffness) and toughness properties, and also because of the superior wetting characteristics of epoxy on natural fibres and improved chemical stability. The epoxy resin type SR 1500 and SD 2505 hardener from Sicomin Epoxy Systems were used, prepared by manual mixing of two components. This particular resin was chosen due to its mechanical properties, demoulding characteristics and excellent adhesion to all types of fibres. The matrix properties are as follows: E = 3.1 GPa, tensile strength σ_f = 74 MPa, strain at maximum load ε_m = 4.4% and failure strain ε_f = 6.0%. The polyurethane adhesive SikaForce® 7888, selected for the bonded joints, was characterized in the work of Neto et al. [15] by bulk tensile tests for the determination of E, σ_f and ε_f, and DCB and ENF tests to define the values of G_n^c and G_s^c, respectively. The obtained results gave E = 1.89±0.81 GPa, σ_f = 28.60±2.0 MPa, ε_f = 43.0±0.6 %, G_n^c = 0.7023±0.1233 N/mm and G_s^c = 8.721±0.792 N/mm.

2.2. Test geometry

The geometry of the DCB specimens is shown in Fig. 1. The dimensions are the total length L = 160 mm, initial crack length $a_0 \approx 50$ mm, laminate thickness h = 5 mm, width B = 15 mm and t_A = 1 mm.

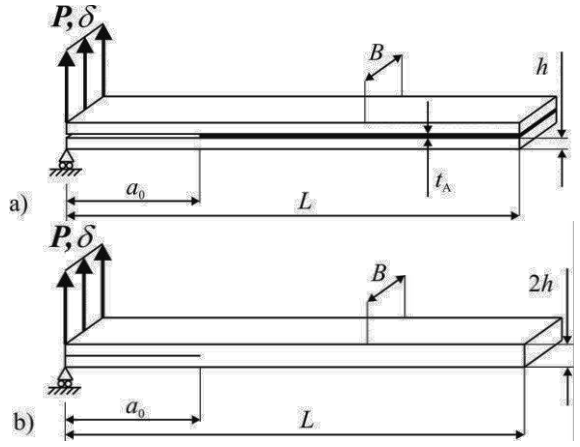

Fig. 1. Geometry of the DCB bonded (a) and co-cured (b) specimens.

The adherends for the bonded specimens were made of jute-epoxy composite plates, consisting of 8 stacked weave plies and a fibre volume fraction of approximately 30%. The plates were fabricated by hand lay-up and cured at room temperature in a vacuum bag. The bonding process included manual abrasion with 220 grit sandpaper, cleaning with a proper degreaser and assembly in a steel mould. For a uniform value of t_A, calibrated spacers of 1 mm were inserted between the adherends. For the calibrated spacer at the crack tip, 3 plies were stacked and glued together (making a total thickness of 1 mm), composed of a 0.1 mm thick razor blade between 0.45 mm spacers, to create a pre-crack. After bonding, the specimens were left to cure before testing. The co-cured specimens were fabricated by hand lay-up of 16 plies of jute weave and by placing a 70 mm length Melinex® Polyester Film with a thickness of 50 μm at the symmetry plane of the plate to produce a pre-crack of approximately 50 mm. Fabrication and curing of the plates were performed identically to the 8-ply plates. For both specimen configurations, a metric scale was glued with cyanoacrylate in both adherends to allow measurement of the crack length (a) and of the input data for the extraction of the J-integral. Six specimens of each configuration were tested at room temperature and 2 mm/min in an electro-mechanical testing machine (Shimadzu AG-X 100) with a load cell of 100 kN. Data recording was carried out at 5 Hz for the load (P) and testing machine grips displacement (δ). Pictures were recorded during the specimens testing with 5 s intervals using a 15 MPixel digital camera. This procedure allowed obtaining a, and the crack tip opening and rotation. The correlation of these values with the P-δ data was carried out by the time elapsed since the beginning of each test between the P-δ curve and each image.

3. Toughness determination

3.1. Co-cured specimens

Three methods were considered to evaluate G_n^c: (1) the Compliance Calibration Method (CCM), based on the Irwin–Kies equation. For this method, cubic polynomials were used to fit the $C = f(a)$ curves for the calculation of $\partial C/\partial a$ (C is the specimen compliance); (2) the Corrected Beam Theory (CBT), taking into account a crack length correction for rotation and deflection of the adherends at the crack tip, calculated by a regression analysis of $C^{1/3}$ versus a data, and (3) the Compliance-Based Beam Method (CBBM), based on an equivalent crack. Owing to the widespread use of these techniques, detailed descriptions are not presented here, although detailed information can be found in reference [16].

3.2. Bonded specimens

3.2.1. Direct method for fracture toughness estimation

The path-independence of the J-integral can be used to extract relations between the specimen loads and the cohesive law of the crack path [17]. Based on the expression for J defined by Rice [18], it is possible to derive an expression for G_n applied to the DCB specimen (assuming that the J-integral gives a measurement of G_n) [19]:

$$G_n = 12\frac{(P_u a)^2}{Eh^3} + P_u\theta_o \quad \text{or} \quad G_n = P_u\theta_p, \qquad (1)$$

where P_u represents the applied load per unit width at the adherends edges, θ_o the relative rotation of the adherends at the crack tip and θ_p the relative rotation of the adherends at the loading line (Fig. 2).

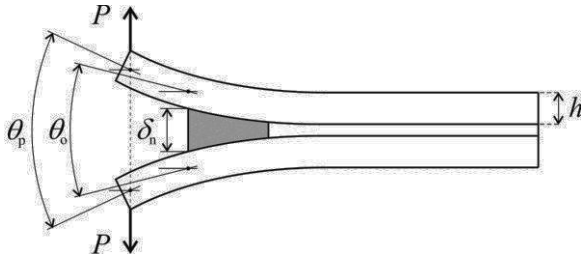

Fig. 2. DCB specimen and analysis parameters.

In this work, the first expression of (1) was considered. The J-integral can be calculated along an

arbitrary path encircling the start of the adhesive layer [17]

$$G_{\mathrm{n}} = \int_0^{\delta_{\mathrm{nc}}} t_{\mathrm{n}}\left(\delta_{\mathrm{n}}\right)\mathrm{d}\delta_{\mathrm{n}}, \qquad (2)$$

where $\delta_{\mathrm{n}}^{\mathrm{c}}$ is the end-opening at failure of the cohesive law (measured at the initial crack tip) and t_{n} is the current normal traction. $G_{\mathrm{n}}^{\mathrm{c}}$ can be considered the value of G_{n} at the beginning of crack growth. Thus, $G_{\mathrm{n}}^{\mathrm{c}}$ is given by the steady-state value of G_{n}, at a δ_{n} value of $\delta_{\mathrm{n}}^{\mathrm{c}}$ [11]. The $t_{\mathrm{n}}(\delta_{\mathrm{n}})$ curve can be easily obtained by differentiation of equation (1) with respect to δ_{n}

$$t_{\mathrm{n}}\left(\delta_{\mathrm{n}}\right) = \frac{\partial G_{\mathrm{n}}}{\partial \delta_{\mathrm{n}}}. \qquad (3)$$

As a result, the procedure of an experiment is to measure the history of P, a, δ_{n} and θ_{o}. The cohesive law in tension can then be estimated by plotting G_{n} in equation (1) or (2) as a function of δ_{n}, polynomial fitting of the obtained curve and differentiation [17].

3.2.2. Optical method for parameter estimation

For calculating δ_{n} and θ_{o} for a given image, the optical method requires the identification of eight points (Fig. 3): two points (p_1, p_2) to measure the current t_{A} value at the crack tip ($t_{\mathrm{A}}^{\mathrm{CT}}$) during loading in image units (pixels), two points (p_3, p_4) identifying a line segment in the image for which the length (d) is known in real world units (mm), two points (p_5, p_6) on the top specimen and two points (p_7, p_8) on the bottom specimen. All eight points are manually identified in the first picture of a trial using an in-house software tool. Using the location of the points in the first picture, the points of the following pictures are automatically identified using a computer algorithm implemented in Matlab. Basically, for each point p_i, a rectangular region centred in p_i is extracted from the first image forming a template (t). This template describes the image pattern that surrounds the point and is used for locating the point in the next image. This is done by finding the position (u,v) in the next image (I) that has the highest normalized cross-correlation with the template, γ [20]. Calculating γ for all the pixels of I results in a matrix, where the maximum absolute value yields the location of the region in I that has the highest correlation with t and, thus, the most likely location of p_i in the next image. This is done for every one of the eight points identified in the first image. After successfully identifying all the points of the second image, new templates are computed from the second image to search for the eight points in the third image, and so on until processing all the images.

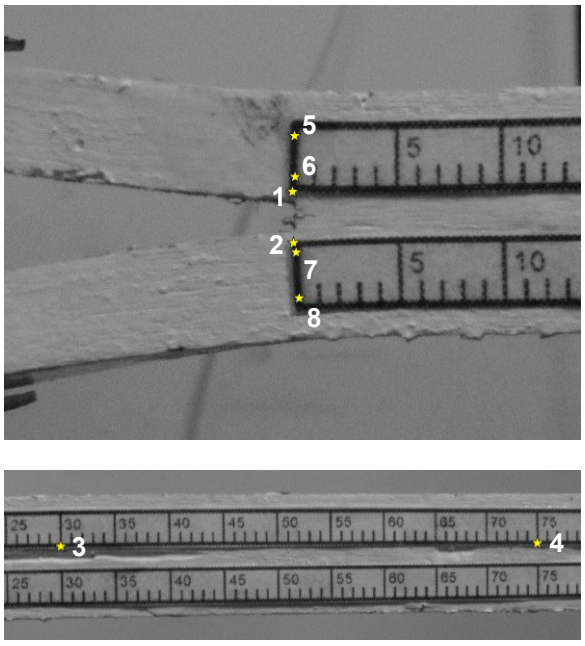

Fig. 3. Points taken by the optical method for measuring θ_{o} and $G_{\mathrm{n}}^{\mathrm{c}}$.

The value of $t_{\mathrm{A}}^{\mathrm{CT}}$ in real world units (mm) is calculated as follows

$$t_{\mathrm{A}}{}^{\mathrm{CT}} = d\frac{\left|p_1 - p_2\right|}{\left|p_3 - p_4\right|}, \qquad (4)$$

assuming that the lens distortion is negligible, which is valid for pictures acquired with modern CCD cameras [21]. Finally, δ_{n} can be defined as

$$\delta_{\mathrm{n}} = t_{\mathrm{A}}{}^{\mathrm{CT}} - t_{\mathrm{A}}, \qquad (5)$$

where t_{A} is the design value of 1 mm. θ_{o} is calculated as the angle between lines l_1 and l_2 (Fig. 4).

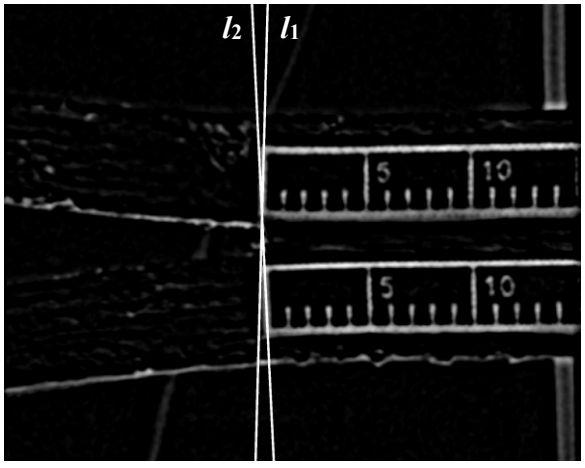

Fig. 4. Image after applying the Difference of Gaussians filter with the lines (l_1 and l_2) that are used to measure θ_{o}.

An image processing algorithm was used to extract the midline of the edge of the ruler. In particular, a Difference of Gaussians filter was applied for enhancing the edges of the ruler, resulting in an image where pixels belonging to edges have high intensity, while the remaining ones have low intensity (Fig. 4). Then, for the rows of the image between p_5 and p_6 (or p_7 and p_8), the midpoint of the edge at each row is computed. This process is repeated for all the rows of each edge of the ruler, resulting in one point per row of the image that define the midline of the edge. Since these points are not necessarily collinear, a linear regression is used for obtaining l_1 (or l_2).

Finally, θ_0 may be calculated as the angle between the two lines

$$\theta_0 = \arccos\left(\frac{\vec{v}_1 \cdot \vec{v}_2}{\|\vec{v}_1\| \cdot \|\vec{v}_2\|}\right) \quad (6)$$

where $\vec{v}_1$ and $\vec{v}_2$ are the direction vectors of lines l_1 and l_2, respectively.

4. Results and discussion

4.1. Co-cured specimens

The interlaminar values of G_n^c were calculated for the co-cured specimens by the previously mentioned techniques. Fig. 5 presents the experimental *R*-curve, relating the evolution of G_n with a, for one tested specimen. Despite this fact, the three methods provide comparable results.

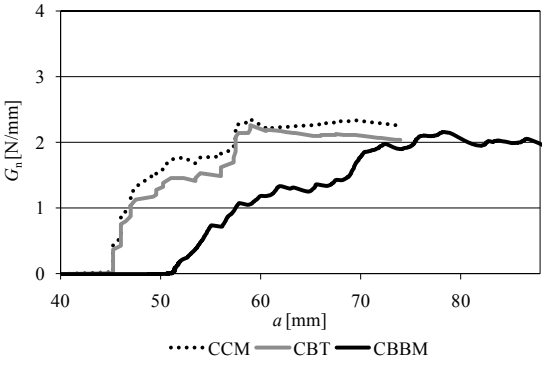

Fig. 5. Experimental *R*-curves for a DCB co-cured specimen.

For the presented specimen, a_0 was measured at 46.25 mm. The value of a_0 for the CBBM corresponded to 54.91 mm, calculated by the first drop of P in the P-δ curve. Disregarding the method, G_n increases from the initiation value, which is related to fibre bridging between the adherends while the crack grows.

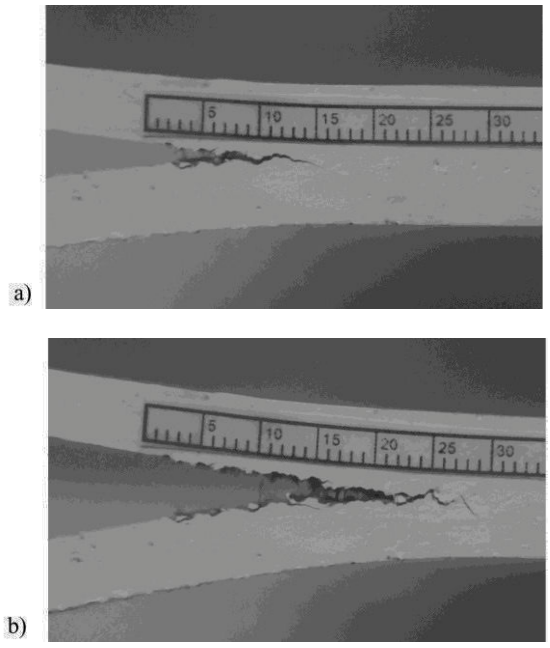

Fig. 6. Crack growth process in a co-cured specimen: before attainment of the steady-state value of G_n (a) and during the steady-state phase (b).

At a G_n value of approximately 2 N/mm, a marked steady-state value of G_n is attained, corresponding to the stabilization of fibre bridging, i.e., balancing between breakage of "older" bridging fibres and creation of new ones at the crack front.

Table 1. G_n^c (N/mm) values of the six co-cured specimens by different methods.

Specimen	Initiation			Stabilization		
	CCM	CBT	CBBM	CCM	CBT	CBBM
1	0.839	0.697	0.716	2.370	1.990	1.685
2	1.330	1.034	0.969	2.103	2.524	2.114
3	1.728	1.274	1.228	2.245	1.973	1.842
4	0.856	0.707	0.745	2.810	1.759	1.655
5	0.625	0.864	0.840	2.615	1.753	1.528
6	1.240	0.750	0.741	2.285	2.105	2.065
Average	1.103	0.888	0.873	2.405	2.017	1.815
St. Dev.	0.405	0.228	0.197	0.261	0.284	0.236

Fig. 6 shows the crack growth process for one specimen during the development of fibre bridging, i.e., before attainment of the steady-state value of G_n (a) and during the steady-state phase (b). Table 1 summarizes the values of G_n^c (N/mm) for the six co-

cured specimens, considering the crack initiation and stabilization values. The agreement between specimens is reasonably good for the CBT and the CBBM, although some deviations occur for the CCM. Between methods, the correspondence is also quite good, especially when comparing the CBT and CBBM.

4.2. Bonded specimens

Initially, θ_0 was estimated by the previously described technique. Fig. 7 exemplifies the evolution of θ_0 for a particular test specimen, which will be used throughout this Section.

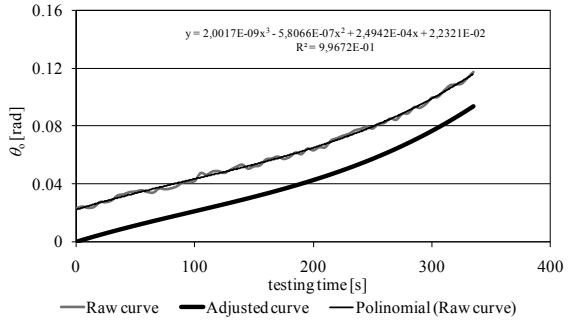

Fig. 7. Evolution of θ_0 for one test specimen: raw curve, polynomial fitting and corrected curve.

The figure represents the raw curve, the 3rd degree polynomial fitting curve to reduce the noise and the corrected polynomial curve, adjusted to make θ_0(testing time=0)=0. In each one of the tested specimens, the most suited degree was selected.

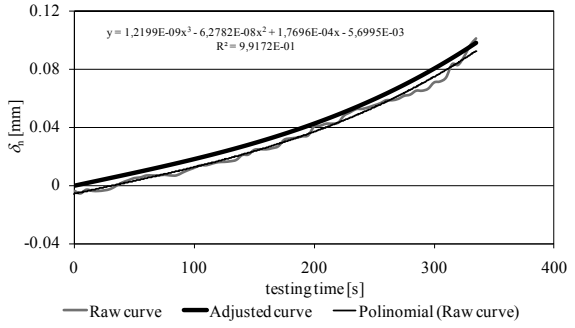

Fig. 8. Evolution of δ_n for one test specimen: raw curve, polynomial fitting and corrected curve.

The polynomial curve adjustment is required to subtract the data from the initial misalignment between glued scales in both adherends. The value of δ_n was also defined for each specimen during testing.

Fig. 8 shows the raw curve from the optical measurements, the polynomial fitting curve and the adjusted curve. The curve shapes in Fig. 7 and Fig. 8 are consistent with the work of Ji et al. [22]. The final adjustment was carried out so that δ_n(testing time=0)=0. The need for this adjustment arises from small deviations to the design value of t_A = 1 mm. The values of G_n^c for the bonded joints were defined by plotting the G_n-δ_n curves, considering G_n^c as the steady-state value of G_n in the G_n-δ_n curve [11]. Fig. 9 plots the experimental G_n-δ_n law and the corresponding polynomial fitting curve. At the beginning of the test, G_n slowly increases with δ_n, but the growth rate of G_n rapidly increases up to nearly δ_n = 0.02-0.04 mm, and a steady-state value of G_n is attained at approximately δ_n = 0.09 mm.

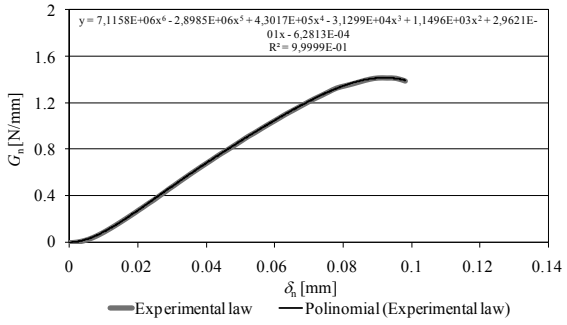

Fig. 9. Experimental G_n-δ_n law for one test specimen and polynomial fitting curve.

For this specimen, the measured value of G_n^c is 1.429 N/mm. The experimental G_n-δ_n law was accurately represented by the fitting polynomial, in a similar fashion to all of the tested specimens (the value of R varied between 0.96 and 0.99). For the six bonded specimens, the obtained data gave $G_n^c = 1.182 \pm 0.215$ N/mm. The reported values for this specific adhesive gave comparable results to previous tests by Neto et al. [15].

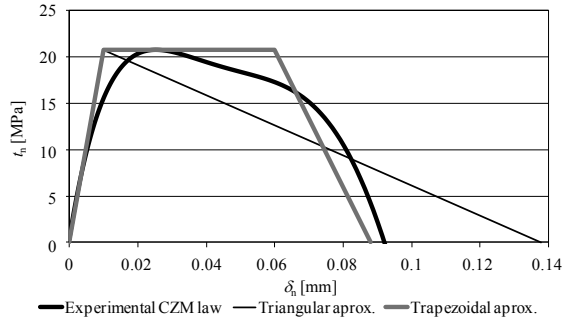

Fig. 10. Experimental t_n-δ_n law for one test specimen.

Fig. 10 shows the obtained experimental t_n-δ_n law, showing the ductile characteristics of the adhesive after the peak value of t_n is attained. For this specimen, the following values were found: t_n^0 = 20.73 MPa and δ_n^c = 0.0935 mm. For the complete batch of tested specimens, average values and deviations were as follows: t_n^0 = 23.18±3.57 MPa and δ_n^c = 0.0843±0.0156 mm. Proposed triangular and trapezoidal simplified CZM laws are also presented, allowing concluding that for the adhesive SikaForce® 7888 a trapezoidal law is particularly suited, since it accounts the best for the adhesive ductility.

5. Conclusions

This work dealt with the determination of G_n^c of adhesive joints between natural fibre composites, either bonding with a ductile polyurethane adhesive or co-curing. G_n^c for the co-cured specimens was estimated by conventional fracture characterization techniques such as the CCM, CBT and CBBM. Results showed consistent *R*-curves between tested specimens and G_n^c values for the three estimation methods. Crack propagation was accompanied by large-scale fibre-bridging, which resulted on crack initiation at $G_n^c \approx 0.9$ N/mm and propagation at $G_n^c \approx$ 2 N/mm, after stabilization of the bridging process. For the bonded joints, the *J*-integral was used to measure G_n^c, given the large adhesive plasticity. An optical measurement and data analysis method was built in Matlab to extract θ_o and δ_n. Average results gave $G_n^c \approx 1.2$ N/mm, proving that at initiation, the bonded joint is tougher than the co-cured joint. However, in a relatively short propagation length, fibre bridging makes the co-cured joint tougher. For the bonded joint, the complete tensile CZM law of the adhesive was derived by the direct method. The CZM curves showed the large plasticity of the polyurethane adhesive. Approximations to triangular and trapezoidal simplified CZM laws showed that the trapezoidal law reproduces the experimental behaviour with a reasonable level of accuracy. As output of this work, the two bonding methods were compared and tensile fracture data was provided for the strength prediction of joints in natural fibre composites by CZM modelling.

References

[1] M.J. Lee, T.M. Cho, W.S. Kim, B.C. Lee, J.J. Lee, *Int. J. Adhes. Adhes.* **30**, 322 (2010).
[2] A.M.G. Pinto, A.G. Magalhães, R.D.S.G. Campilho, M.F.S.F. de Moura, A.P.M. Baptista, *J. Adhesion* **85**, 351 (2009).
[3] T.H. Kim, J.H. Kweon, J.H. Choi, *J. Reinf. Plast. Compos*. **27**, 1071 (2008).
[4] J.M. Ferreira, H. Silva, J.D. Costa, M. Richardson, *Compos.: Part B* **36**, 1 (2005).
[5] S. Varghese, B. Kuriakose, S. Thomas, *J. Appl. Polym. Sci.* **53**, 1051 (1994).
[6] P. Wambua, J. Ivens, I. Verpoest, *Compos. Sci. Technol*. **63**, 1259 (2003).
[7] D. Plackett, The natural fiber-polymer composite industry in Europe-technology and markets. Proceedings of the Progress on Woodfibre-Plastic Composites Conference 2002, University of Toronto, Toronto, Canada, 2002.
[8] L.F.M. da Silva, R.D.S.G. Campilho, Advances in Numerical Modelling of Adhesive Joints, Springer, Heidelberg, 2011.
[9] C.D.M. Liljedahl, A.D. Crocombe, M.A. Wahab, I.A. Ashcroft, *Int. J. Fract.* **141**, 147 (2006).
[10] R.D.S.G. Campilho, M.F.S.F. de Moura, A.M.G. Pinto, J.J.L. Morais, J.J.M.S. Domingues, *Compos.: Part B* **40**, 149 (2009).
[11] T. Carlberger, U, Stigh, *J. Adhesion* **86**, 814 (2010).
[12] H. Ku, H. Wang, N. Pattarachaiyakoop, M. Trada, *Compos.: Part B* **42**, 856 (2011).
[13] T. Schloesse, J. Knothe, *Kunststoffe. Plast. Europe* **87**, 25 (1997).
[14] P.J. Roe, M.P. Ansell, *J. Mater. Sci.* **20**, 4015 (1985).
[15] J.A.B.P. Neto, R.D.S.G. Campilho, L.F.M. da Silva, *Int. J. Adhes. Adhes.* **37**, 96 (2012).
[16] M.D. Banea, L.F.M. da Silva, R.D.S.G. Campilho, *J. Adhes. Sci. Technol.* **26**, 939 (2012).
[17] U. Stigh, K.S. Alfredsson, T. Andersson, A. Biel, T. Carlberger, K. Salomonsson, *Int. J. Fatigue* **165**, 149 (2010).
[18] J.R. Rice, *J. Appl. Mech.* **35**, 379 (1968).
[19] M.D. Banea, L.F.M. da Silva, R.D.S.G. Campilho, *J. Adhes. Sci. Technol.* **24**, 2011 (2010).
[20] J.P. Lewis, Fast Template Matching, Vision Interface 95, Canadian Image Processing and Pattern Recognition Society, Quebec City, Canada, May 15-19, 1995, p. 120-123.
[21] Z. Zhang, Camera calibration, in Emerging Topics in Computer Vision, G. Medioni and S. Kang, Eds. Prentice Hall Professional Technical Reference, 2004, ch. 2.
[22] G. Ji, Z. Ouyang, G. Li, S. Ibekwe, S.S. Pang, *Int. J. Solids Struct.* **47**, 2445 (2010).